HHS Public Access

Author manuscript

Conf Proc IEEE Eng Med Biol Soc. Author manuscript; available in PMC 2017 August 08.

Published in final edited form as:

Conf Proc IEEE Eng Med Biol Soc. 2016 August ; 2016: 6250–6253. doi:10.1109/EMBC.2016.7592157.

Effects of Coplanar Shielding for High Field MRI

Joseph V. Rispoli [Member, IEEE],
Biomedical Engineering Department, Texas A&M University, College Station, TX 77843 USA. He is now with the Weldon School of Biomedical Engineering, Purdue University, West Lafayette, IN 47907 USA

Matthew D. Wilcox,
Biomedical Engineering Department, Texas A&M University

Samantha By,
Biomedical Engineering Department, Texas A&M University. She is now with the Biomedical Engineering Department, Vanderbilt University, Nashville, TN 37215 USA

Steven M. Wright [Fellow, IEEE], and
Biomedical Engineering Department and Electrical Engineering Department, Texas A&M University

Mary P. McDougall [Member, IEEE]
Biomedical Engineering Department and Electrical Engineering Department, Texas A&M University

Abstract

This work investigates the efficacy of "coplanar shielding," in which copper shields are oriented concentric and coplanar to the RF coils rather than implemented as a full ground plane behind them. Following FDTD simulations to determine optimal shielding parameters, two coil geometries were constructed: a circular loop surface coil and a half-volume five-element receive array. Each was evaluated using bench measurements with and without coplanar shielding. Imaging, including accelerated SENSE imaging, was performed with the shielded and unshielded receive arrays on a whole-body 7T scanner. Results from modeled and fabricated coils showed good agreement with improvements in Q factors for all cases. Imaging showed substantial improvements in SNR and g-factors for the coplanar shielded array.

I. Background

Radiative and dielectric tissue losses account for a more significant share of radiofrequency (RF) coil loss [1]–[3] at higher field strengths. Adding RF shields is a standard approach to alleviate B_0-dependent radiative losses and becomes increasingly compelling at higher fields [4]. Adriany et al. characterized the performance of a variety of 7T surface coils using conventional shielding; results demonstrated appreciable benefits for shielded coils over

phone: 765-494-6178; fax: 765-496-1459; jrispoli@purdue.edu.

unshielded versions, prompting the authors to categorically recommend RF shields for coils larger than 7 cm [5].

A variety of shielding methods have been explored as alternatives to typical copper sheeting. One such scheme adds concentric conductors around each coil; variations of this method have been shown to reduce radiative losses, inter-element coupling, and load-induced frequency shift, while also limiting flux blockage from other elements [6–11]. A simple implementation, dubbed coplanar shielding, encircles the coil with a continuous copper loop. This scheme, in contrast to other concentric shielding approaches, maintains the ability to overlap array elements. Preliminary results with a single-loop surface coil indicated a coplanar shield improved the coil filling factor and reduced total coil loss at 7 T, thus improving transmit efficiency [10].

II. Methods

A. Electromagnetic Modeling

The effects of coplanar shielding on various performance metrics were analyzed with full-wave electromagnetic modeling. Simulations were performed using commercial FDTD software (Remcom XFdtd® 7.4). Coils with mean diameters of 8 cm and 16 cm were modeled; for each case a single coil was centered at the origin on the xz plane. Two coil conductor configurations were modeled for each diameter: printed circuit board (PCB) and wire. The PCB trace was meshed as a two-dimensional sheet (4-mm width for 8-cm coil, 6-mm width for 16-cm coil), while wire was modeled as a three-dimensional revolved solid with a circular cross section (18 AWG/0.5-mm radius for 8-cm coil, 12-AWG/1-mm radius for 16-cm coil).

The shield width and coil-to-shield spacing were parameterized in XFdtd, and QtScript macros were developed to construct 100 combinations of shield width and spacing, in 1-mm steps from 1–10 mm. The coplanar shield was meshed as a two-dimensional sheet. The unshielded case was also simulated for each coil geometry. All conductors were assigned the electrical properties of copper (σ = 59.6 MS/m, ε_r = 1). Load spacing was simulated at one distance to mimic 1-cm padding present in coils utilized for in vivo studies. A slab measuring 32 × 32 × 20 cm was centered and spaced 1 cm below the coil and assigned the electrical properties of muscle at 7 T (σ = 0.55 S/m, ε_r = 80).

All coils included equally-spaced, 2-mm wide breaks (six for 8-cm coil, 12 for 16-cm coil) to accommodate the feed and segmentation capacitors. Capacitor values for each simulation were assigned to produce uniform current around the loop, and capacitor definitions included a 0.2-Ω resistance to model ohmic losses from equivalent series resistance and solder resistivity [12].

The two PCB coils and 12-AWG wire coil were gridded with maximum 1-mm Yee cell dimensions, while the 18-AWG wire coil was gridded with maximum 0.5-mm dimensions. For all cases, the mesh was excited by a broadband pulse and simulations converged when transients dissipated to levels −50 dB below peak values. Grid convergence was verified using a 0.25-mm grid spacing for specific geometries. A surface conductor correction was

applied to copper planes to ensure conductivity consistent with five skin depths. XFdtd's conformal meshing algorithm for curved objects was applied to all conductors. For all cases, the model was surrounded by a quarter wavelength of free space padding cells, and the boundary comprised seven perfectly matched layers. The ROI of the coil was defined as the hemisphere below the loop. Three planar sensors captured steady-state B- and E-field data at 298 MHz, the Larmor frequency at 7 T. The circuit components, i.e., feeds and capacitors, recorded both transient and steady-state data. Resulting sensor data were imported into MATLAB for postprocessing. FDTD results from selected shielding geometries were validated against in-house full-wave spectral-domain analysis code [13] by comparing calculated input impedance, current uniformity, and field patterns over the uniform loading phantom.

The quality factor Q was calculated from an initial round of FDTD simulations where each was capacitor replaced by an ideal current source at the capacitor break. All other performance metrics were determined with modeled capacitors at each break and a single 50Ω voltage source across the feed. The input impedances (with resistance R and reactance X) were summed and Q-factors were calculated from Eq. (1):

$$Q=\omega L/R=X/R \quad (1)$$

Here R includes ohmic capacitor losses. SNR was determined from the average $|\mathbf{B}_1^-|$ in the ROI divided by $\sqrt{R_{\text{in}}}$ at the feed. Transmit efficiency was calculated by dividing the average $|\mathbf{B}_1^+|$ in the ROI by the square root of power dissipated from combined ohmic, radiative, and tissue losses. Average $|\mathbf{E}|/|\mathbf{B}_1^+|$ in the ROI was computed to assess sample losses due to E fields. Local SAR was gauged by the ratio of computed $|\mathbf{E}|_{\text{max}}^2/|\mathbf{B}_1^+|$ throughout the coil's ROI.

Finally, radiation efficiency was determined as the proportion of power radiating into the mesh boundary to total power; if the model includes a sample load, this metric excludes radiation dissipated in the sample; it should be noted that most power radiating out of the FDTD mesh would ultimately dissipate in the subject due to confinement by the magnet bore and magnet room RF screen [14].

B. Radiofrequency Coils

A single circular loop surface coil was constructed and evaluated with three shielding topologies—coplanar shielded, ground plane shielded, and unshielded. The surface coil was etched on 1.6-mm thick, 1-ounce copper-clad FR-4 PCB with 16-cm mean diameter and 6-mm conductor width. The coil was segmented by 12 equally-spaced 2-mm breaks. A coplanar shield with 7-mm conductor width and 176-mm inner diameter (resulting in 5-mm spacing between coil and shield) was fabricated for placement around the loop coil. Simulations results indicated this shield spacing was optimal, and the width was selected as wider traces yielded diminishing improvements, as discussed further in Section III-A. The ground plane shielded case was evaluated by orienting a copper sheet 4.5 cm below the surface coil, a separation previously determined to be best suited for surface coils of this size [5]. Capacitors values of 10 and 12 pF (Passive Plus) were utilized for the unshielded and

shielded cases, respectively. The coils were loaded with a 28-cm diameter, 14-cm tall cylindrical saline phantom (σ = 0.55 S/m). Each coil was evaluated in unloaded and loaded conditions, with all cases balanced matched to 50 Ω with variable capacitors (SGNMNC1206E, Sprague-Goodman; NMAJ55HVE, Voltronics). *Q*-factors were measured with a network analyzer (Keysight E5071C) based on the −7 dB width of the S_{11} response [15].

Shown in Fig. 1, a custom “Olympic rings” array of five overlapping elements was constructed to compare coplanar-shielded and unshielded parallel imaging performance. Each element was shaped from 18-AWG wire formed into an 8-cm diameter loop and segmented into six equal arcs. The resulting gaps were connected by ceramic chip capacitors (100B series, American Technical Ceramics; 1111C series, Passive Plus). Elements were mounted on a half-cylindrical acrylic former with a 78-mm radius. A standard active trap configuration incorporating the match capacitor, variable solenoid (164 series, Coilcraft), and PIN diode (MA4P7470F-1072, MACOM) detuned the array elements during transmit. Additional protection was provided midway around the loop by a passive trap incorporating dual anti-parallel diodes and the tune capacitor.

Inter-element decoupling was accomplished via optimal geometric overlap for nearest neighbors, and all elements utilized low-input impedance preamplifier decoupling [16]. Standard resonant cable traps were included at each element’s feed. For the shielded array, each wire element was encircled by a coplanar shield etched on 0.2-mm thick, 1-ounce copper-clad FR-4 PCB with 89-mm inner diameter and 97-mm outer diameter; again, the coplanar shield geometry was designated after considering the various simulated performance metrics. Each individual element’s coplanar shield remained electrically isolated by affixing insulating polyimide tape between overlapping conductors.

The half-volume arrays were loaded with a cylindrical 1-gallon saline phantom, with conductivity of muscle at 7 T (σ = 0.55 S/m), spaced 10 mm from the conductors. *Q*-factor measurements were performed using the procedure described above for the surface coil. Imaging was performed on a whole-body 7T scanner (Achieva, Philips Medical Systems) with the receive array and phantom positioned inside a commercial quadrature transmit head coil (Nova Medical). A 3D T1 High-Res Isotropic Volume Excitation (THRIVE) sequence was utilized with 4-ms TR, 1.83-ms TE, 8° flip angle, 1-mm isotropic resolution throughout an 18 × 18 × 32 cm FOV. Array performance was evaluated from resulting images by comparing SNR. To gauge accelerated imaging performance, bidirectional SENSE scans [17] were executed with reduction factors of up to R = 3 in the phase-encoding direction (right/left—RL) and up to R = 2 in the frequency-encoding direction (feet/head—FH). The resulting coil geometry factors (g) were calculated and illustrated as g-factor maps on a coronal slice through the phantom.

III. Results

A. Electromagnetic Modeling

Simulation results suggest, regardless of coil size, a specific coil-to-shield spacing exists that optimizes transmit efficiency for any particular dielectric load at a given B_0. Furthermore, a

qualitative comparison confirmed the aforementioned metrics are in agreement for wire and PCB coils with equivalent mean diameters. Still, optimizing transmit efficiency comes at the expense of other metrics, including SNR and local SAR. Thus, the design decision is ultimately a tradeoff between several performance metrics.

Modeling results of transmit efficiency for the two constructed coil types are shown in Fig. 2. The results suggest that for muscle imaging at 7 T, transmit efficiency peaks when the coplanar shield's inner radius is spaced 8 mm from the mean coil diameter, with wider shield widths delivering diminishing improvements. A 10-mm wide shield is expected to provide 28% (2.1 dB) improvement in $|\mathbf{B}_1^+|$ efficiency against the unshielded case. In general, increasing the coplanar shield width increases transmit efficiency and SNR and reduces the average E field in the sample, while increasing shield spacing from the coil increases $|\mathbf{B}_1^+|$ homogeneity. All shielded cases improved the ratio of average $|\mathbf{E}|/|\mathbf{B}_1^+|$ compared to the unshielded case, indicating proportionately reduced losses from the E field. The radiation efficiency is quite low with the large muscle load at 7 T; instead, the majority of coil losses originate from the dB/dt-induced non-conservative E field. Notably, the $|\mathbf{E}|_{max}^2/|\mathbf{B}_1^+|$ results indicated a potential increase in peak local SAR of up to 25% depending on shield geometry.

B. Radiofrequency Coils

As shown in Table 1, the coplanar shielded configuration of the 16-cm surface coil exhibited a twofold higher loaded Q-factor (Q_l) as compared to the unshielded and ground plane shielded cases. The unloaded-to-loaded Q ratios (Q_{ul}/Q_l) greater than two for all cases indicate losses from the sample dominate, as desired, in the loaded case. Given the higher loaded Q-factor for the coplanar shielded coil, the power required to achieve a given B_1 with this load is expected to be roughly half that required with the unshielded coil.

Elements from the 8-cm shielded and unshielded arrays exhibited loaded Q-factors of up to 28 and 8.1, respectively. The magnitude of these values are in close agreement with the simulated Q-factors of 31 and 9.4. Furthermore, the resulting shielded-to-unshielded Q ratios are within 5% when comparing bench measurements and simulations. Together, these data support the validation of simulation results with and without coplanar shields.

With phantom imaging at 7 T, the shielded array provided a 23% improvement in mean SNR throughout the top half (7-cm depth) of the cylindrical phantom. Fig. 3 displays SNR maps for the two arrays on an axial slice through the phantom.

Results from SENSE-accelerated imaging indicate the arrays perform similarly at lower bidirectional reduction factors and $R = 2$ in the phase-encoding direction (RL). However, with threefold reduction ($R = 3$) in the RL direction the coplanar-shielded array dramatically outperformed the unshielded array, with 64% and 85% the unshielded max and mean g-factors. Notably, at bidirectional $R = 6$ the shielded array exhibited a mean g-factor of 1.19, within the regime ($g < 1.2$) considered to be favorable for accelerated imaging [18]. The g-factor maps for both arrays on the coronal plane at 7-cm depth in the phantom are shown in Fig. 4.

IV. Conclusion

Coplanar shields have been shown to improve coil Q and transmit $|\mathbf{B}_1^+|$ efficiency. Furthermore, while it has been reported that non-overlapped elements improve SENSE imaging SNR by means of higher g-factors despite additional coupling and basic noise [19], coplanar shielding recoups some of the reported performance deficits of overlapped elements, all the while maintaining the an array's ability to maximize SNR through conventional parallel imaging.

Supplementary Material

Refer to Web version on PubMed Central for supplementary material.

Acknowledgments

Research supported by CPRIT RP100625 and NIH EB016394.

The authors thank Ivan Dimitrov and Sergey Cheshkov for assistance imaging with the array coils.

References

1. Vaughan JT, et al. 7T vs. 4T: RF power, homogeneity, and signal-to-noise comparison in head images. Magn Reson Med. Jul; 2001 46(1):24–30. [PubMed: 11443707]
2. Keltner JR, et al. Electromagnetic fields of surface coil in vivo NMR at high frequencies. Magn Reson Med. Dec; 1991 22(2):467–480. [PubMed: 1812380]
3. Vaughan, JT. Ultra high field MRI: high-frequency coils. In: Robitaille, P-M., Berliner, LJ., editors. Ultra high field magnetic resonance imaging. New York: Springer; 2006. p. 127-161.
4. Ong KC, et al. Radiofrequency shielding of surface coils at 4.0 T. J Magn Reson Imaging. Nov; 1995 5(6):773–777. [PubMed: 8748501]
5. Adriany, G., et al. Shielded surface coils and halfvolume cavity resonators for imaging and spectroscopy applications at 7 tesla. Proc. 8th Annu. Meeting ISMRM; 2000; p. 563
6. Belliveau JG, Gilbert KM, Abou-Khousa M, Menon RS. Analysis of circumferential shielding as a method to decouple radiofrequency coils for high-field MRI. Concepts Magn Reson Part B: Magn Reson Eng. Feb; 2013 43B(1):11–21.
7. Gilbert KM, et al. A conformal transceive array for 7 T neuroimaging. Magn Reson Med. May; 2012 67(5):1487–1496. [PubMed: 22190335]
8. Gilbert KM, Curtis AT, Gati JS, Klassen LM, Villemaire LE, Menon RS, et al. Transmit/receive radiofrequency coil with individually shielded elements. Magn Reson Med. Dec; 2010 64(6):1640–1651. [PubMed: 20648678]
9. Lanz, T., Griswold, M. Concentrically shielded surface coils—a new method for decoupling phased array elements. Proc. 14th Annu. Meeting ISMRM; 2006; p. 217
10. McDougall, MP., et al. A printed loop element with integrated capacitors and co-planar shield for 7 tesla. Proc. 19th Annu. Meeting ISMRM; 2011; p. 1875
11. El-Khair, IA., Korvink, JG., Hennig, J., Moenich, G. The shielding of RF MRI coils using double-sided EMI shield. Proc. 17th Annu. Meeting ISMRM; 2009; p. 105
12. Kumar A, Edelstein WA, Bottomley PA. Noise figure limits for circular loop MR coils. Magn Reson Med. May; 2009 61(5):1201–1209. [PubMed: 19253376]
13. Wright SM. Full-wave analysis of planar radiofrequency coils and coil arrays with assumed current distribution. Concepts Magn Reson. Mar; 2002 15(1):2–14.
14. Liu W, Kao CP, Collins CM, Smith MB, Yang QX. On consideration of radiated power in RF field simulations for MRI. Magn Reson Med. Jan; 2013 69(1):290–294. [PubMed: 22473620]

15. Doty F, Connick T, Ni X, Clingan M. Noise in high-power, high-frequency double-tuned probes. J Magn Reson. May; 1988 77(3):536–549.
16. Roemer P, Edelstein W, Hayes C, Souza S, Mueller O. The NMR phased array. Magn Reson Med. Nov; 1990 16(2):192–225. [PubMed: 2266841]
17. Pruessmann KP, Weiger M, Scheidegger MB, Boesiger P. SENSE: sensitivity encoding for fast MRI. Magn Reson Med. Nov; 1999 42(5):952–962. [PubMed: 10542355]
18. Wiesinger F, et al. Parallel imaging performance as a function of field strength—an experimental investigation using electrodynamic scaling. Magn Reson Med. Nov; 2004 52(5):953–964. [PubMed: 15508167]
19. Weiger M, Pruessmann KP, Leussler C, Röschmann P, Boesiger P. Specific coil design for SENSE: A six-element cardiac array. Magn Reson Med. Mar; 2001 45(3):495–504. [PubMed: 11241709]

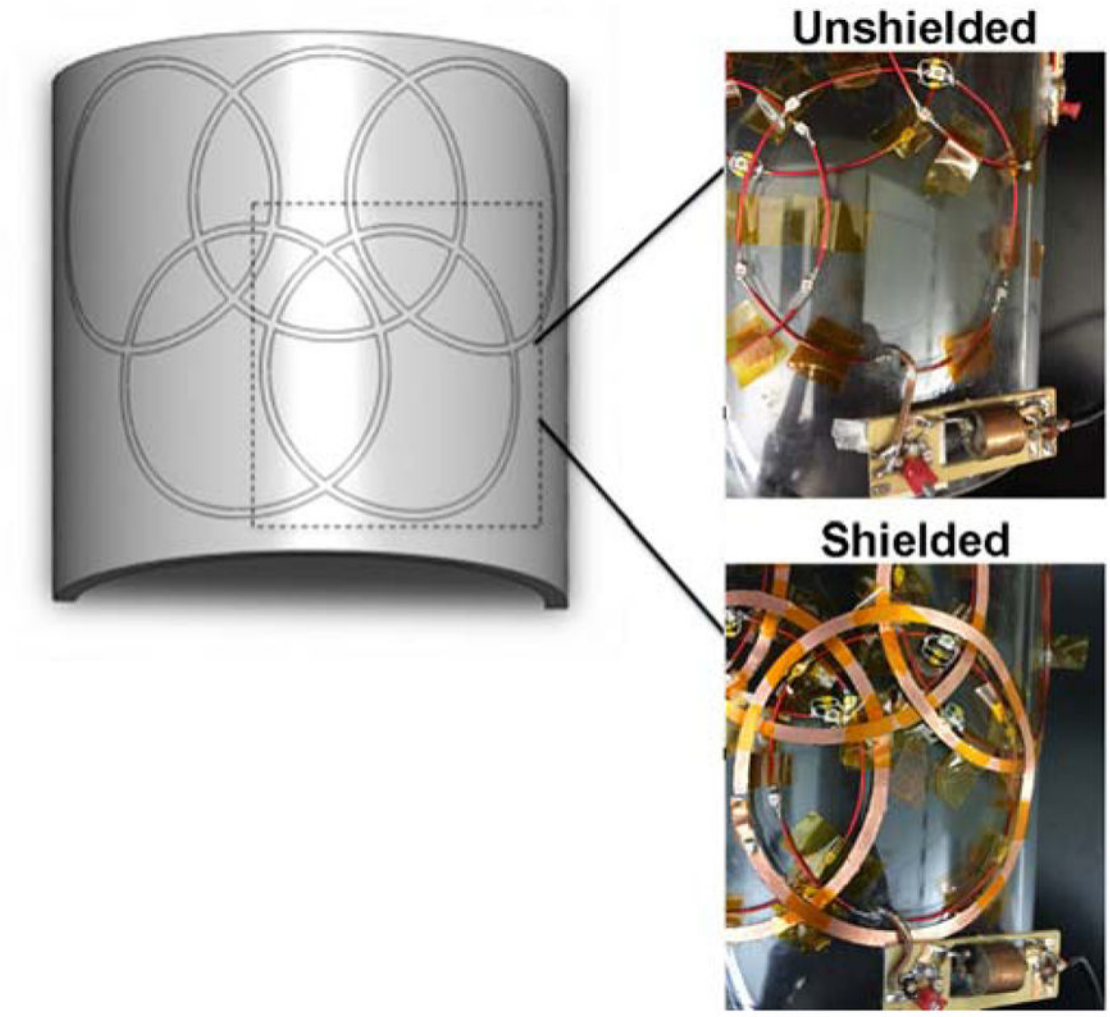

Figure 1.
3D rendering and photographs of “Olympic rings” array coils.

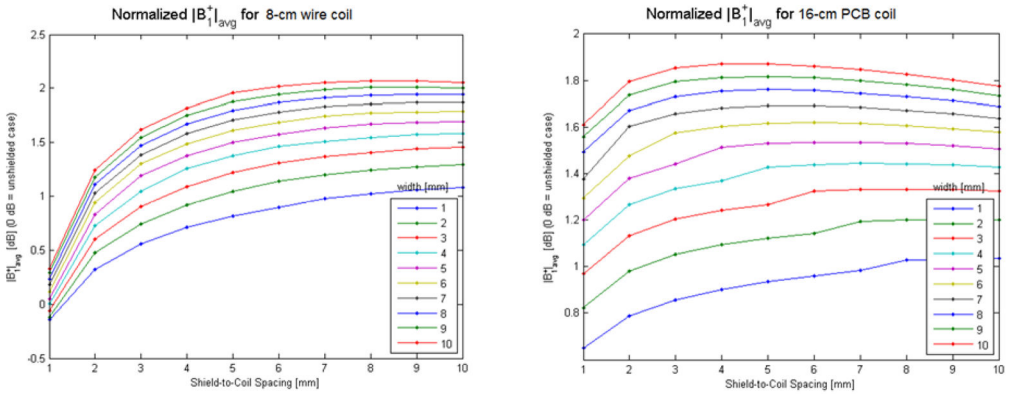

Figure 2.

Normalized $|\mathbf{B}_1^+|$, an indicator of transmit efficiency, for the 8-cm wire (left) and 16-cm PCB (right) coplanar shielded loop coils. Both plots have been normalized to 0 dB = the unshielded case. Note the 16-cm coil had a conductor width of 6 mm so, for example, a shield-to-coil spacing of 1 mm is equivalent to 4 mm spacing between the shield and center of the coil conductor.

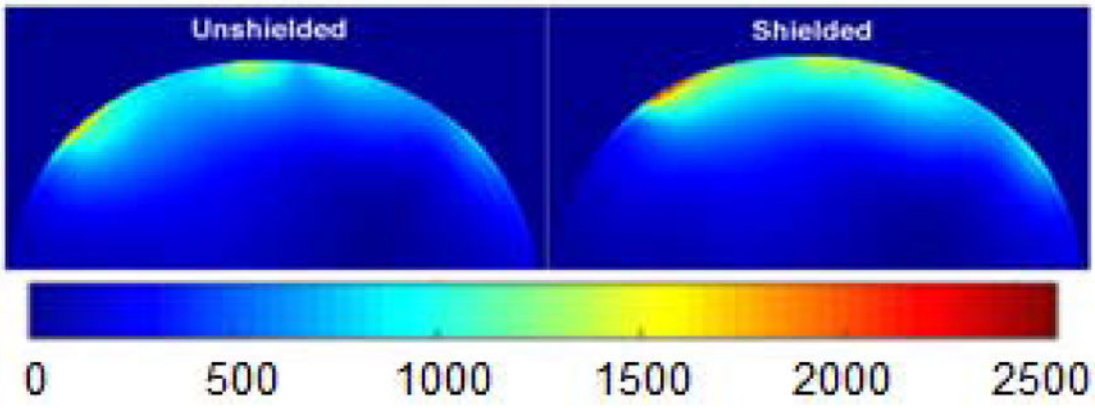

Figure 3.
Axial view of SNR maps from shielded and unshielded array coils.

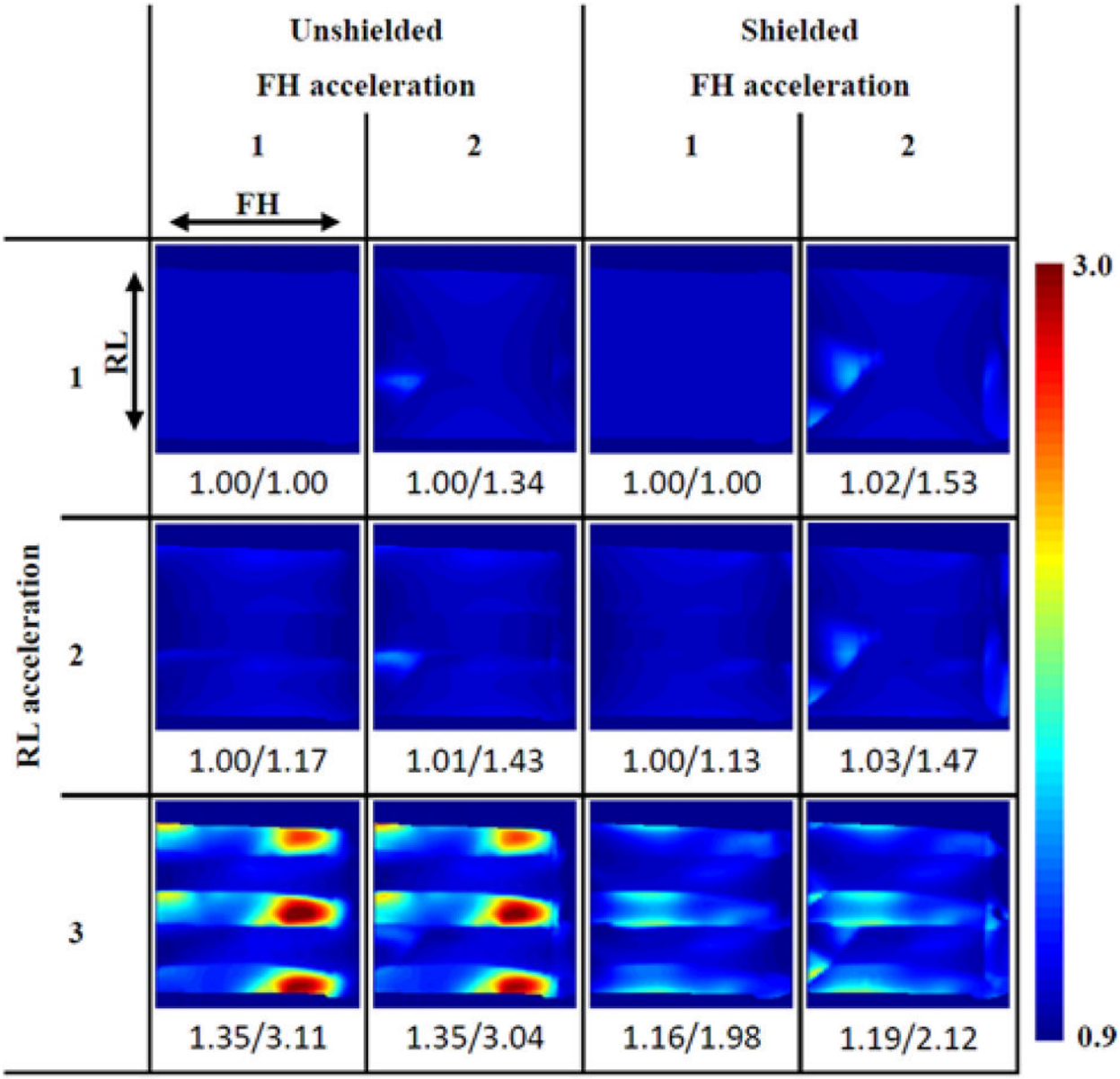

Figure 4.

g-Factor maps from bidirectional SENSE-accelerated scans. Values indicate mean and maximum *g*-factors for each case. The shielded array exhibits significantly lower g-factors with three-fold RL acceleration.

Table 1

Q-factor comparison of the 16-cm loop coil with various shield configurations

Shielding Configuration	Q_l	Q_{ul}	Q_{ul}/Q_l
Unshielded	4.4	52	12
Coplanar shielded	11	130	12
Ground plane shielded	5.1	200	39